Track-Scale Simulations of Selective Laser Melting to Investigate Development and Mitigation of Thermal Stresses

Rahul Sharma[1] · Arvind Kumar[1] (ID)

Abstract

This work investigates the evolution of thermal stresses, dependence of residual stress on important process parameters, critical locations of high stresses and ways to minimize them by adopting the appropriate set of the parameters for selective laser melting of Ti6Al4V at track-scale. A fully coupled 3D thermo-mechanical model is developed. Elasto-plastic material and material properties considered are dependent on temperature. In the coupled modelling approach, the validation of thermal model carried out with the available experimental data. Detailed analysis of temperature field and resulting thermal stresses is then presented. During heating, compressive stress zone is observed in the neighbourhood of the melt pool and balancing tensile stress zone below it. As laser traverses forward, tensile stresses are generated in the solidified melt pool region and a balancing compressive stress zone underneath it is observed. It is quantified that with increase in laser heat source power and interaction time, the magnitude of residual stress increases, but pre-heating the substrate reduces the residual stress. The magnitude of residual stress is also decreased by adopting the alternate-scan strategy over the uni-directional scan-strategy. Apart from delineating the detailed quantitative analysis of residual stress, this work helps understand the evolution of thermal stress in the SLM process at the fundamental level, i.e. at track-scale which is the basic building block. This understanding is crucial to control the residual stresses at part scale. Volume reduction during the conversion of powder material to bulk liquid has been received less attention in the previous thermal models. Thus, its incorporation in the present thermal model makes the modelling approach more realistic, as the predictions of the thermal model act as important inputs to the coupled mechanical model that calculates stresses.

✉ Arvind Kumar
  arvindkr@iitk.ac.in

  Rahul Sharma
  rahulsh@iitk.ac.in

[1] Department of Mechanical Engineering, Indian Institute of Technology Kanpur, Kanpur 208016, India

Nomenclature

A	Laser absorptivity of the powder material
C_p	Specific heat capacity (J kg^{-1} K^{-1})
h	Convective heat transfer coefficient (W m^{-2} K^{-1})
k	Thermal conductivity (W m^{-1} K^{-1})
L	Latent heat of the fusion (J kg^{-1})
P	Laser power (W)
q	Heat energy from the laser beam (W m^{-2})
R	Laser beam radius (m)
T	Temperature (K)
t	Time (s)
v	Velocity of laser (m/s)

Greek Symbols

ϕ	Porosity of the powder layer
ρ	Density (kg m^{-3})
β_T	Coefficient of thermal expansion of liquid (K^{-1})
ε'	(Emissivity)
σ'	Stefan Boltzmann constant (W m^{-2} K^{-4})
β	Volume fraction of liquid phase
α_m	Mass fraction
α	Coefficient of thermal expansion of solid (K^{-1})

Subscripts

l	Liquid
s	Bulk solid
p	Powder
$solidus$	Solidus temperature
$liquidus$	Liquidus temperature
ref	Reference
$conv$	Convection
rad	Radiation

Introduction

Over the years, the additive manufacturing technology has gained popularity by evolving from rapid prototyping to manufacturing of actual parts. As reported by Dutta and Froeas [1], initially additive manufacturing technique is used mainly in aerospace and automotive sector but nowadays it is popular in every industry. It requires careful control of processing conditions right from the beginning of the process, i.e. the CAD model development in the design software to the end of the process, i.e. the post processing on manufactured parts. Gokuldoss et al. [2] reported that among the various additive manufacturing processes, Selective Laser Melting (SLM), which is a powder-

bed-fusion based technique, is popular owing to its capability to manufacture high density parts. Gibson et al. [3] reported that in SLM layer-by-layer scanning is done till the whole component is manufactured. Titanium alloy (Ti-6Al-4 V) has suitable applications in aerospace industry but is a costly material. Ahmad et al. [4] indicated that for this material, large material wastage in conventional machining process shifted the focus to this process using SLM where little material wastage occurs, and less final machining is required. Though, the SLM technique has many advantages, such as near net shape component, high density parts, negligible waste etc., it has some disadvantages also. Leuder et al. [5] concluded that the material properties of product manufactured by SLM are directly related to its microstructure and which depends on the thermal load during the process. Vastola et al. [6] states that the thermal residual stress is one of the main problems in SLM manufactured component which leads to defects, such as cracking, bending and distortion in the component and reduced strength of the component due to change in microstructure. Therefore, understanding the evolution of the thermal residual stress in the component manufactured by SLM process is important. A thorough quantitative analysis can help to devise methods to reduce it.

Shiomi et al. [7] reported a theoretical model for the deposition of powder layer over substrate in selective laser melting. Using the model, the effect of heat treatment, substrate heating and re-scanning of the track on relieving the residual stress was studied. It reported that heat treatment for one hour to 600 °C, substrate heating to 160 °C and re-scanning of the track relives 70%, 40% and 55% stresses, respectively. Mercelis and Kruth [8] developed a theoretical model to evaluate the stress field in the component manufactured by selective laser sintering and selective laser melting. The restricted expansion of the upper layer due to large amount of heat input caused thermal stress during heating stage, and inhibited shrinkage of the top layer during the cooling stage caused thermal stress during cooling stage. The effect of number of layers, yield strength of the material and base plate height was studied by using an experimental approach. They reported that the residual stress was increased with increase in number of layers deposited, increase in yield strength of the material and decrease in the base plate height. Cheng et al. [9] studied the residual stress with variation in scanning strategies, such as island scanning, line scanning, 45° line scanning, 45° rotate scanning, 90° rotate scanning, 67° rotate scanning, in-out scanning and out-in scanning. They reported that 45° line scanning has minimum residual stress while out-in scanning pattern has maximum residual stress. Also, the part deformation was found minimum in the 45° line scanning. Similarly, Song et al. [10] studied the effect of scanning strategies by considering two different mechanical boundary conditions. They observed that the scanning strategy has great influence on temperature field but negligible effect on melt pool size. Also, 15° rotate scan strategy generated the minimum stress among the all studied scan strategies. Hussein et al. [11] presented a 3D non-linear sequentially coupled thermo-mechanical model to predict temperature field, melt pool dimensions and resulting thermal stresses. They observed the highest temperature gradient at the start of the first track scan, which in result induces the highest von Mises stress in that region. The tensile stress zone was found in the solidified melt pool and compressive stress zone in the surrounding of tensile zone to balance it. Li et al. [12] proposed a temperature-thread multiscale modeling approach to predict the distortion and residual stress in a part. The temperature field required to melt powder was estimated in the

microscale scan model. Then, it was applied to the mesoscale model directly, and finally, the thermal field of one block of hatch layers was transported to the macroscale model. The total computational time was reduced using the multiscale approach. Li et al. [13] also used this technique for fast prediction of part distortion for different scan strategies. Li et al. [14] investigated the thermal field evolved during the selective laser melting (SLM) process with a moving volumetric heat source. The volume shrinkage due to change in the density of the material during phase change is incorporated in the model, which is more realistic modelling approach. It was found that with high laser power and low scanning speed, the length, width and depth of the melt pool increases. But, due to exclusion of vaporisation of the material in the model, there is over-estimation of the melt pool size. Tan at al. [15] developed the thermo-metallurgical-mechanical coupled model to study the temperature, solid-state phase and residual stress fields for the multi-track multi-layer selective laser melting process of Ti6Al4V by using the solid-state phase transformation (SSPT). They found that by using SSPT, there is decrease in tensile residual stresses and increase in compressive residual stresses due to decrease in material volume during the heating process and increase in volume during the cooling process, which is different from the thermal expansion and contraction caused by the temperature change, and also the residual stress component in the longitudinal direction is larger than the other two stress components.

The thermal residual stress in the component manufactured by selective laser melting technique restricts its potential for commercial use. It becomes very important to choose appropriate parameters and build strategy in order to reduce the residual stress while building a component by SLM. Despite the advancements in additive manufacturing field, the available literature discusses the residual stress at macro-scale but the origin and evolution of thermal stress at fundamental level (track-scale) is not addressed comprehensively. Since track-scale is the basic building block of the layered fabrication, it is crucial to understand the origin of the thermal stresses and its evolution during the processing in order to devise effective strategies to minimize the unwanted residual stress development. The experimental study for the evolution of thermal stress at fundamental level of track-scale is very challenging as it requires well-controlled conditions and experimental analysis tools. Therefore, computational studies that carefully consider the attendant physical phenomena will be very effective as an alternate tool. In this study, a track-scale 3D thermo-mechanical model is developed to investigate the temperature field and the thermal stress developed during the processing of Ti6Al4V powder layer by the SLM technique. Using the developed model, micro-scale and meso-scale studies are performed. The model considers melting and solidification phase change, temperature dependent material properties, volume shrinkage of the porous powder layer upon its melting and further re-solidification, and elasto-plastic behaviour of the material. The incorporation of volume shrinkage of the porous powder layer upon its melting and further re-solidification in the numerical model is more realistic approach and studied only in a few literature [14, 15]. Micro-scale study is carried out for single layer single track scanning to investigate the evolution of temperature field and resulting thermal stress. The high residual stress locations are determined. Subsequently, the effect of important parameters, such as laser power, substrate pre-heat temperature and laser scanning speed on the resulting residual stress is described in the micro-scale study. Thereafter, a meso-scale study is performed for single layer muti-track scanning to understand the effect of alternate and

uni-directional scan strategy on the resulting residual stress. In the end, stress development in single layer multi-track build is minimized by adopting the optimum parameters obtained from the present study.

Mathematical Model

A fully coupled thermo-mechanical model is developed for analysing the evolution of temperature field and resulting thermal stress at the fundamental track-scale level, Firstly, to understand the development of thermal field and resulting thermal stresses, a micro-scale study is performed in which scanning of single track single powder layer of Ti6Al4V is considered over the solid substrate of Ti6Al4V. A 540 μm × 200 μm × 200 μm solid substrate is considered over which a powder layer of 540 μm × 200 μm × 30 μm is laid over (Fig. 1 (a)). Only half of the domain is simulated to save on simulation time, thanks to symmetry in x-z plane. The domain dimensions were selected after running several simulations at different dimensions and observing when the computed temperatures became nearly independent of the domain size. There are three modes of heat transfer in the computational domain. Radiative and convective losses are accounted from the top boundary while heat transfer from powder layer to the rest of the domain takes place through conduction. The value of convective heat transfer coefficient is taken as 40 W m^{-1} K^{-1} [16], while the ambient temperature is taken as 293 K. Except for the top surface and plane of symmetry, all other boundaries of the domain are considered adiabatic. It can be noted that a small amount of heat transfer can take place from substrate to the gas present in the chamber. But, because of very small time involved in single track scanning there will be little time available for heat diffusion up to the boundaries. Also, there is no indication in the available literature how to incorporate this heat loss and the value of heat transfer coefficient for chamber cooling at the substrate boundary. Therefore, in absence of such information, a simplified approach, as also used by Wu et al. [17], is adopted, and such heat losses are not considered. After micro-scale study, a meso-scale study is performed to study the effect of scanning strategy on thermal residual stress by scanning single layer multi-track powder layer laid over the solid substrate. For this a solid substrate of dimensions 540 μm × 400 μm × 20 μm with a powder layer of dimensions 540 μm × 200 μm × 30 μm is taken (Fig. 1 (b)). The process parameters used in the all simulations are tabulated in Table 1. In the end, a numerically quantified demonstration is delineated to minimize the residual stress field developed by choosing a set of the appropriate parameters, as suggested in this study.

Material Properties

Due to localized heating during the SLM process, there will be localized high temperature zone in the domain. Therefore, consideration of temperature dependent material properties is very important. Tables 2 and 3 show the thermal properties of Ti6Al4V, and the mechanical properties are listed in Table 4. In simulations the temperature dependent material properties were linearly interpolated in between the given data.

The properties of the powder layer are defined by considering it as a homogeneous material. To incorporate powder layer porosity in the numerical model, the following relationships were used [22]:
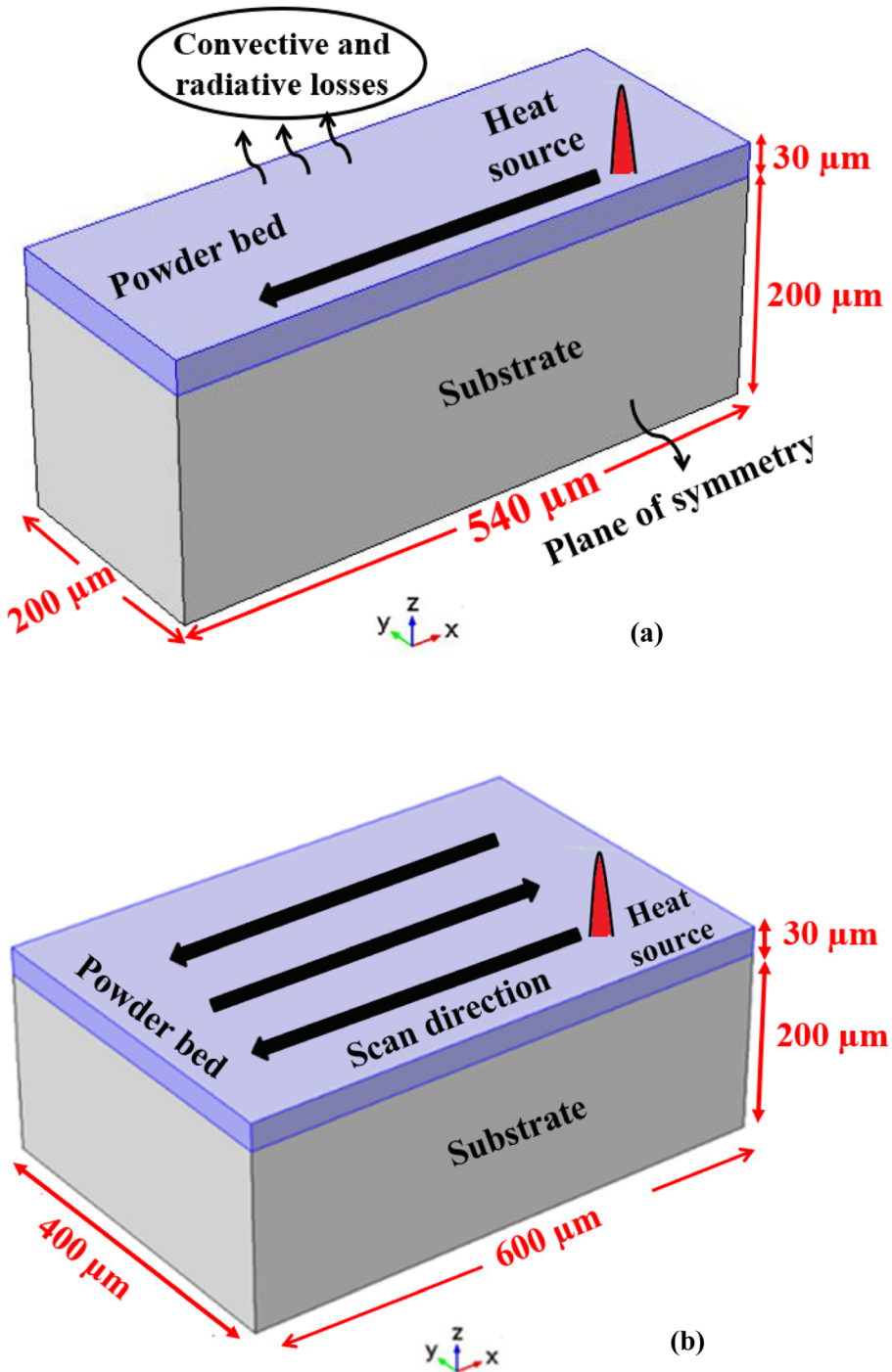
Convective and radiative losses

Heat source

30 μm

Powder bed

200 μm

Substrate

540 μm

Plane of symmetry

200 μm

z
y   x

(a)

Heat source

30 μm

Powder bed

Scan direction

200 μm

Substrate

400 μm

600 μm

z
y   x

(b)

Fig. 1 Schematic of (a) computational domain for micro-scale model (b) computational domain for meso-scale model

Table 1 Process parameters used in simulations

Parameters	Value
Laser power	40 W
Laser absorption coefficient	0.4
Laser spot radius	26 μm
Laser scanning speed	250 mm/s
Hatch spacing	50 μm

Table 2 Thermo-physical properties of Ti6Al4V [18–20]

Solidus temperature (K)	1877	
Liquidus temperature (K)	1923	
Density of bulk solid (kg m^{-3})	$4512 - (0.154 \times T)$	$293 < T \le 1923$ (T in K)
Density of the liquid (kg m^{-3})	4122	
Specific heat of bulk solid (J kg^{-1} K^{-1})	$483.04 + (0.215 \times T)$ $412.7 + (0.1801 \times T)$	$T \le 1268$ (T in K) $1268 < T \le 1923$ (T in K)
Specific heat of liquid (J kg^{-1} K^{-1})	831	
Latent heat of fusion (kJ kg^{-1})	286	
Thermal conductivity of bulk solid (W m^{-1} K^{-1})	$1.2595 + (0.0157 \times T)$ $-12.752 + (0.024 \times T)$	$T \le 1268$ (T in K) $1268 < T \le 1923$ (T in K)
Thermal conductivity of liquid (W m^{-1} K^{-1})	$-12.752 + (0.024 \times T)$ (T in K)	

Table 3 Emissivity value for powder and solid Ti6Al4V [21]

Temperature (K)	Emissivity
293	0.121
373	0.155
473	0.178
573	0.205
673	0.228
773	0.331
873	0.561
973	0.591
1173	0.600
1773	0.600
1923	0.405
2173	0.402
2373	0.400
2573	0.398
2879	0.395

Table 4 Mechanical properties of Ti6Al4V [21]

Temperature (K)	Coefficient of thermal expansion × 10⁻⁶ (1/K)	Young's modulus (GPa)	Yield strength (MPa)	Plastic tangent modulus (GPa)
293	8.78	125	1000	0.7
367	9.83	110	630	2.2
478	10.0	100	630	2.2
590	10.7	100	525	2.2
701	11.1	80	500	1.9
812	11.2	74	446	1.9
923	11.7	55	300	1.9
1034	12.2	27	45	2
1145	12.3	20	25	2
1367	12.4	5	5	2
1923	12.5	0.3	0.3	0.3

$$k_P = k_S \frac{(1-\phi)}{(1 + 11\phi^2)} \tag{1}$$

$$\rho_P = \rho_S(1-\phi) \tag{2}$$

where ϕ is the porosity of the powder layer (taken as the typical value of 0.35). Typically, the powder layer and melt pool do not possess any rigidity but for the convergence of the mechanical model, a small negligible value of 0.3 GPa is considered in the simulations.

Numerical Implementation

Simulation Methodology

The numerical model developed for the analysis of thermal stress has two components, i.e., the thermal model and the mechanical model. The two models are fully coupled at each time step. At each time step, firstly, the thermal model is solved by incorporating appropriate boundary conditions to evaluate the temperature field in the whole domain. Then, the temperature field is coupled with the mechanical model by converting thermal load on the domain into equivalent mechanical load at the same time step. The stress field in the domain is obtained by using mechanical boundary conditions at same time step. This procedure is repeated for each time step. The flowchart of the modelling scheme is displayed in Fig. 2.

Model Setup

For the pre-processing and analysis of the stresses in the computational domain, a FE model is established in COMSOL Multiphysics software. The computational domain is divided into two parts, i.e., a solid substrate and the powder bed. In order to perform micro-
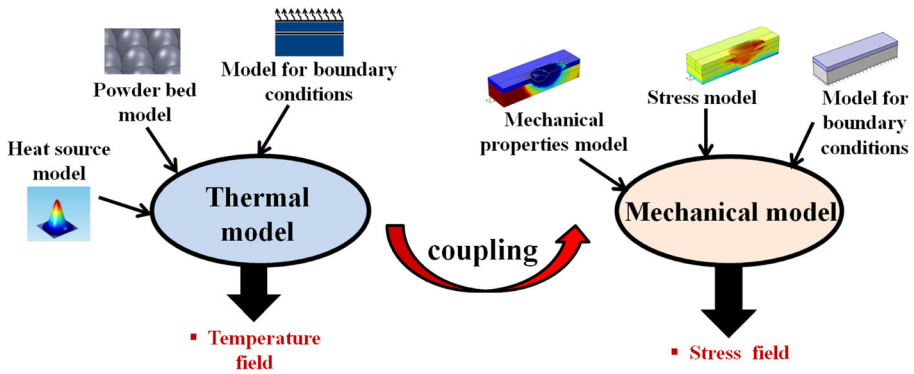
Fig. 2 Flowchart of thermo-mechanical coupling

scale analysis, the computational domain is meshed with fine mesh in the laser interacted powder layer and substrate region, whereas the remaining domain is meshed with coarse mesh. Grid independent test is performed before reporting the final results, and a mapped mesh with the maximum size of 12 μm (length) × 12 μm (width) × 10 μm (height) gives the grid independent result in the laser interaction region. There are 405 elements in the laser interacted powder layer region and total of 2295 elements in the whole computational domain. For the meso-scale analysis, powder layer is meshed with mapped mesh with the size of 12 μm (length) × 12 μm (width) × 10 μm (height) with total of 4500 elements in the powder layer and the remaining domain has coarse mesh with total of 2900 elements.

Thermal Model

In SLM, localized heating in the powder layer occurs by laser heating. The heat gained by powder layer is transmitted to the surrounding in the form of radiative and convective losses from the top surface and rest of the heat energy being dissipated in the domain by conduction. As a result, a temperature field develops in the domain.

Energy conservation equation is given as

$$\frac{\partial(\rho C_P T)}{\partial t} = \nabla \cdot (k \nabla T) \tag{3a}$$

where ρ, and k in the powder bed are defined as

$$\rho = (1-\beta)\rho_{phase\ 1} + \beta\rho_{phase\ 2} \tag{3b}$$

$$\beta = \begin{pmatrix} 0 & T < T_{solidus} \\ \dfrac{T-T_{solidus}}{T_{liquids}-T_{solidus}} & T_{solidus} \leq T \leq T_{liquids} \\ 1 & T \geq T_{liquids} \end{pmatrix} \tag{3c}$$

$$C_p = \frac{1}{\rho}\left((1-\beta)\rho_{phase1}C_{p,phase\ 1} + \beta\rho_{phase2}C_{p,phase\ 2}\right) + L\frac{\partial \alpha_m}{\partial T} \tag{3d}$$

$$\alpha_m = \frac{1}{2} \frac{\beta \rho_{phase2} - (1-\beta) \rho_{phase1}}{(1-\beta) \rho_{phase1} + \beta \rho_{phase2}} \tag{3e}$$

$$k = (1-\beta) k_{phase1} + \beta k_{phase2} \tag{3f}$$

Here β is a linear function indicating the fraction of phase before transition, and α_m is the mass fraction. The function β varies between 0 and 1. Its value as zero represents region having temperature lower than $T_{solidus}$ and its the value as one represents the region having temperature more than $T_{liquidus}$. Further, *phase1* represents solid phase which includes the substrate, the solidified melt pool and the powder layer, while *phase2* represents liquid phase. The value of C_p of the bulk solid and the powder bed are assumed to be equal.

For prescribing the initial condition in the model, the whole domain is at the room temperature ($T_{ref} = 293$ K). The heat input through Gaussian type laser heat source is incorporated through boundary condition as follows:

$$k \frac{\partial T}{\partial n} = q - q_{conv} - q_{rad} \tag{4a}$$

where q is the laser heat source energy, and q_{conv} and q_{rad} are convective and radiative losses, respectively.

$$q = \frac{2AP}{\pi R^2} exp \left(-\frac{2(x-vt)^2}{R^2} \right) \tag{4b}$$

$$q_{conv} = h \left(T - T_{ref} \right) \tag{4c}$$

$$q_{rad} = \varepsilon' \sigma' \left(T^4 - T_{ref}^4 \right) \tag{4d}$$

where A is the absorption coefficient, P is the laser heat source power, v is the laser scanning velocity, h is the convective heat transfer coefficient and ε' is the emissivity of the powder and solid material.

Volume Reduction of the Powder Layer

When the whole powder layer is scanned by laser the newly deposited layer will appear raised on the solid substrate. But, during scanning of a single track in the powder layer, when the solidified track is observed along with the adjacent sidewise and frontwise powder it will appear depressed, owing to the volume reduction in the powder layer upon melting (see Fig. 3). The powder layer over the substrate is porous due to presence of voids. When the porous layer, is operated by the laser heat source, powder converts to bulk melt and the initial
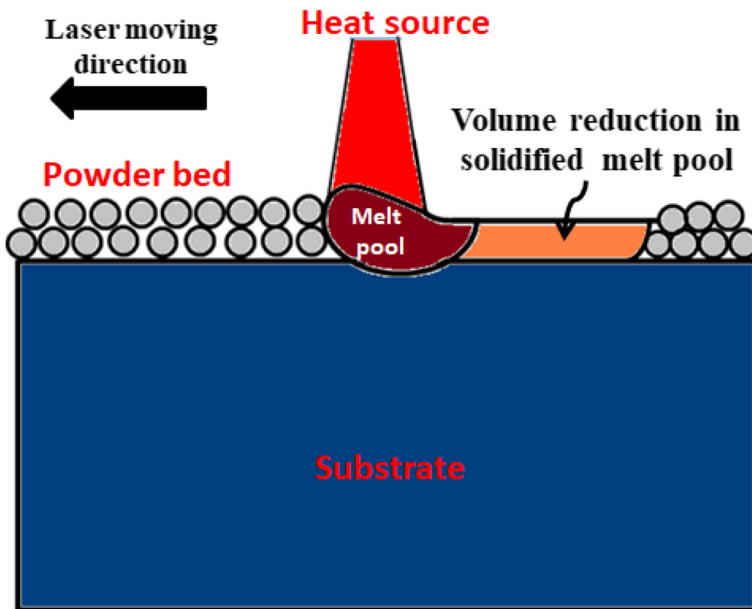
Fig. 3 Volume reduction upon melting in the porous powder layer

voids present in the layer seep out. Therefore, density of the bulk melt is more than the density of the powder layer. Since, the mass of the powder layer is conserved, the increase in the density of the material upon melting will cause decrease in the volume of the melted and solidified layer, as shown in Fig. 3. To incorporate this strategy, the deformed geometry physics in COMSOL Multiphysics™ software has been used. This enables the motion of the boundary of the computational domain with time. A time-dependent downward displacement of the top surface of the melt pool is incorporated as soon as the melting starts [23]. It is to be noted that in the results discussed subsequently, the results are shown along with the adjacent powder; therefore the melt pool and the solidified track will appear as they are sinking in the powder.

Mechanical Model

At each time step, the thermal model is coupled with the mechanical model and the temperature field obtained acts as equivalent force for the mechanical model which in result gives the stress field. The computational domain has several small cells. For each cell, the model relating the force and the displacement is described as [17]:

$$\{dF\}^e + \{dR\}^e = [K]^e\{d\delta\}^e \tag{5}$$

where $\{dF\}^e$ is elemental force incremental vector of a mesh cell, $\{dR\}^e$ is the equivalent force increment caused by temperature change in the each element, $[K]^e$ is the elemental stiffness matrix and $\{d\delta\}^e$ is the incremental displacement

vector. For the whole domain, the stiffness matrix and force increment vector is given as

$$[K] = \sum \{dK\}^e \tag{6}$$

$$\{d\mathbf{F}\} = \sum (\{d\mathbf{F}\}^e + \{d\mathbf{R}\}^e) \tag{7}$$

There is no external force applied on the domain and only source of stress generation is the temperature field. Therefore,

$$\sum \{d\mathbf{F}\}^e = 0 \tag{8}$$

The force–displacement relation is given as

$$\{d\mathbf{F}\} = \sum \{d\mathbf{R}\}^e = [\mathbf{K}]\{d\boldsymbol{\delta}\} \tag{9}$$

The elemental strain is calculated through elemental strain-displacement relation as

$$\{d\varepsilon\}^e = [\mathbf{B}] \{d\boldsymbol{\delta}\}^e \tag{10}$$

where $[\mathbf{B}]$ is the matrix related to elemental strain vector.

The stress-strain constitutive law is given as

$$\{d\boldsymbol{\sigma}\} = [\mathbf{D}]\{d\varepsilon\} \tag{11}$$

where $[\mathbf{D}]$ is the elastic-plastic stiffness matrix.

The initial and boundary conditions are expressed as

$$\{d\varepsilon\}(x, y, z, t)|_{(t=0)} = 0 \ (x, y, z, t \in \mathbf{R}) \tag{12}$$

$$\{d\varepsilon\} \ (x, y, z, t)|_{(z=0)} = 0 \ (x, y, z, t \in \mathbf{R}) \tag{13}$$

Results and Discussion
Thermal Model Validation

Temperature gradient is the driving mechanism for the development of thermal stress in selective laser melting process. Therefore, to ensure accuracy of the thermal model, the predicted results were compared with the experimental results of Verhaeghe et al. [24]. The predicted melt pool width and substrate melting depth for single layer single track scan for the cross-section perpendicular to laser scanning direction at different laser power ranging from 20 W to 80 W are validated (see Fig. 4). The process parameters
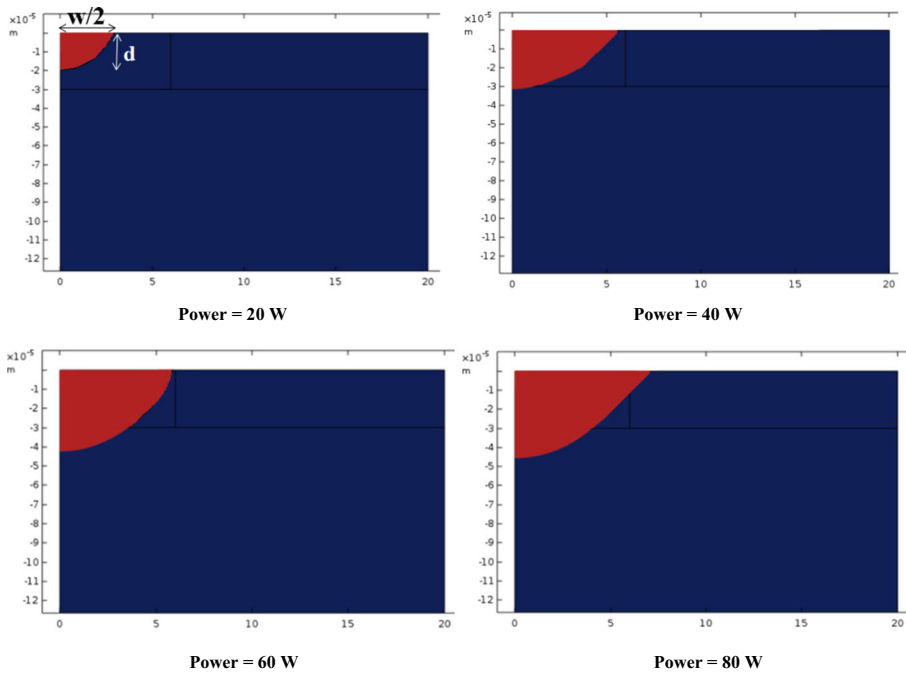
(a)
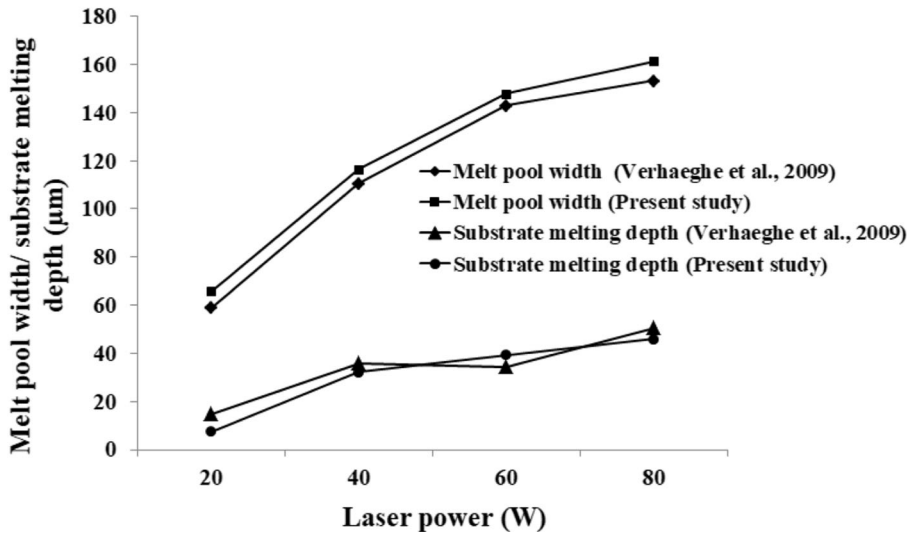
(b)

Fig. 4 **(a)** Liquid-solid phase field in the y-z cross section of the powder bed and substrate at various laser heat source power **(b)** comparison of the predicted and the experimental melt pool width and substrate melting depth variation with laser heat source power

(i.e., scanning speed = 200 mm/s and beam radius = 30 μm) were kept same as those in the experimental study of Verhaeghe et al. [24]. The evaporation of the material is not considered.

It can be noted that this work focuses on the evolution of thermal stress at the track-scale during scanning of single powder layer by SLM. At this scale, there is requirement of controlled experiments to measure the evolution of stress. However, no experimental data is available in literature for stress evolution for single layer single track scanning. Therefore, there is no possibility to directly validate the simulated stress filed. Hence, an indirect approach is followed, i.e., the thermal model, which serves as the main input for the mechanical model, is validated. As temperature gradient is the cause of thermal stress, therefore, validation of thermal model is necessary to predict correct stress field. After obtaining a good comparison of the simulated melt pool width and substrate melting depth with the experimental results, the thermal model is considered validated, and then further investigations on the track-scale thermal stress are carried out.

Single Track Laser Scan Simulations for Micro-Scale Stress Evolution

To understand the development of thermal field and resulting thermal stresses during the single-track scanning in SLM, simulation is performed at micro-scale, i.e., on single layer single track scanning of powder layer. A 40 W laser heat source having spot radius of 26 μm with Gaussian type intensity disruption is used with scanning speed of 250 mm/s. Figure 5 shows the temperature maps during heating, solidification of the melt pool and cooling period. The powder layer is scanned by the laser heat source up to 1750 μs (heating stage), after this time it is cooled down up to 4000 μs (cooling stage). The maximum temperature reaches up to 4710 K. During the scanning, melt pool expands to the substrate depth and some melting there also takes place which is required to make good bonding between the newly deposited layer and the solid substrate. Volume reduction of the scanned layer takes place due to removal of voids present in between the loosely held powder particles upon melting and solidification and is seen as a dip in the scanned powder layer adjacent to the un-processed powder layer (Fig. 5). After the completion of the cooling stage, i.e., at 4000 μs, the top layer is allowed to cool down above the ambient temperature up to 550 K. This is because in the SLM process before the deposition of new layer, the previous layer remains pre-heated up to some temperature above the ambient temperature which also reduces thermal stress [25–27]. Therefore, in the present model, the previously deposited layer is not allowed to cool completely up to the ambient temperature.

During the SLM process, two phase change process occur in the powder layer, from powder to liquid state and then from liquid state to bulk solid. The value of the material properties also changes with different phases of the material. Therefore, it is important to incorporate the change of the material properties with the different phase of the material. Figure 6 shows the material properties variation in the model with different phase of the material. As shown in Fig. 6 (a), the unprocessed powder has density of the powder material, the laser interacted region has density of the liquid and the already scanned region has density equivalent to the bulk solid. Similarly, other material properties, such as yield strength and Youngs modulus vary as phase change of the material takes place.
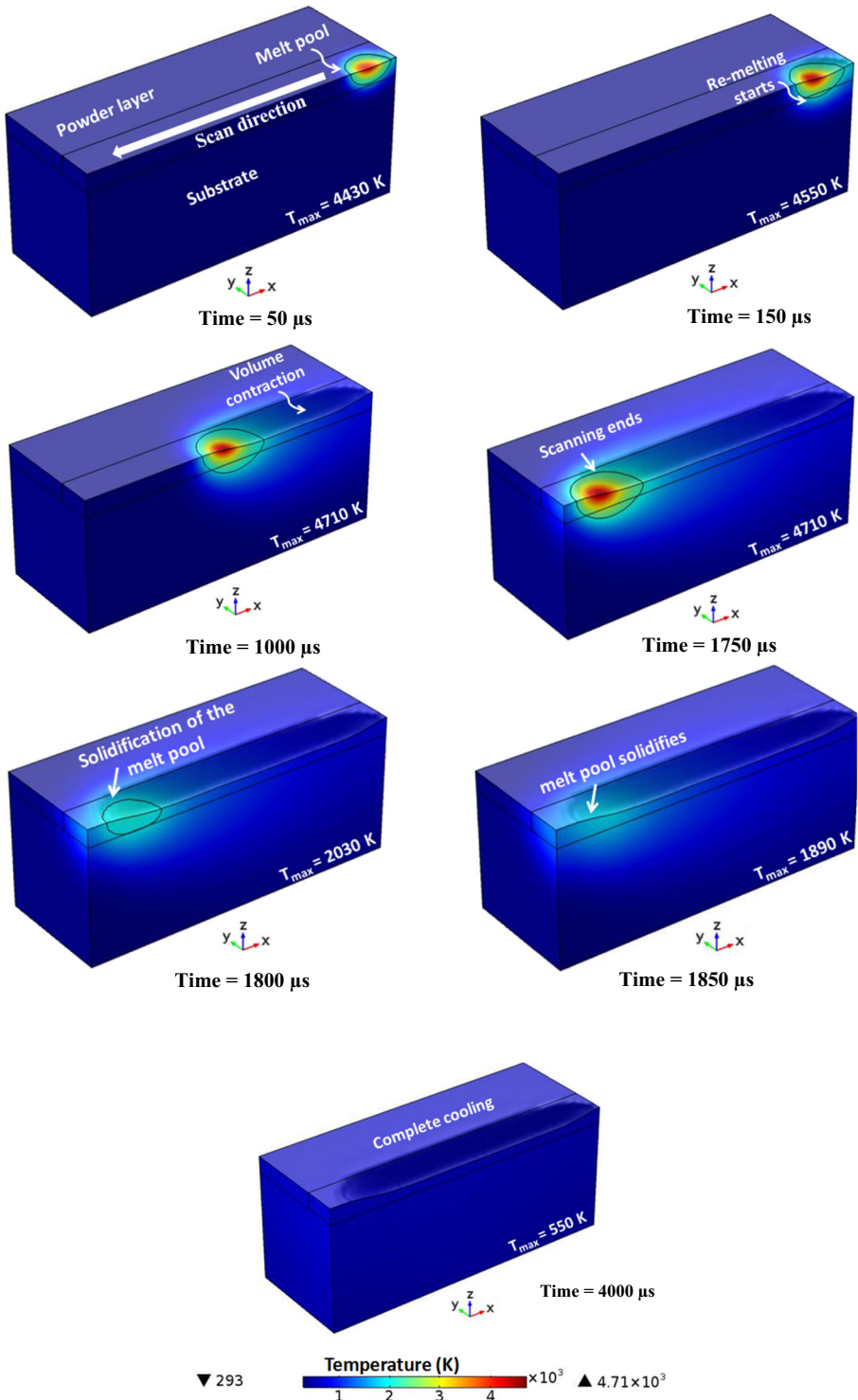
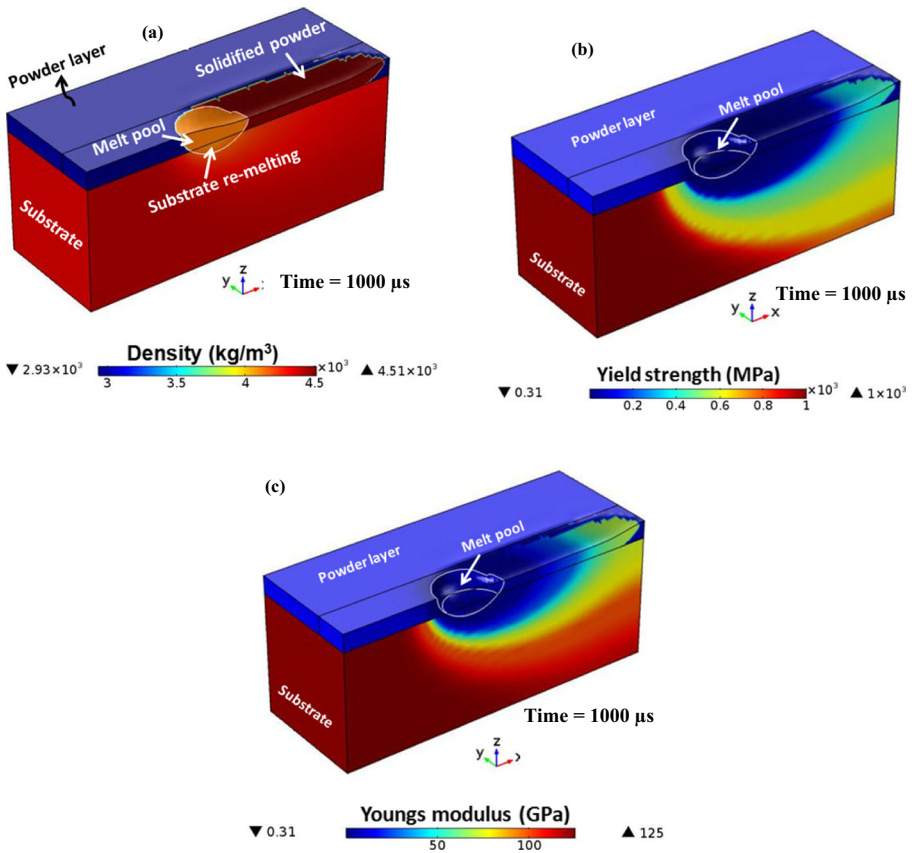Fig. 5   Temperature maps during heating and cooling stages

Fig. 6 (a) Density map (b) yield strength map (c) Youngs modulus map during laser scanning

Stresses during heating of the component

Figure 7 (a) presents the stress field (σ_{xx}) during the heating of the component at time 1000 μs and 1750 μs. There is a zone of compressive stress from the neighbouring region of melt pool to the depth of 115 μm of the solid substrate. This is because the neighbouring material of melt pool tries to expand after gaining heat from the melt pool, but the surrounding material does not allow it to expand freely. Hence, compressive stress developed in the neighbourhood of melt pool. It is worth to note that the zone of high compressive stress is present at some distance away from the melt pool. This is because high temperature in the neighbourhood of the melt pool results in loss of material's rigidity and hence less magnitude of stresses. There is a tensile stress zone present below the compressive stress zone to balance it and hence maintains the equilibrium. The already scanned layer experiences the tensile stress as shown in Fig. 7 (a). This is because when the laser heat source moves forward, top layer of the material cools down and starts shrinking. But the surrounding material restricts the free contraction of the top layer due to which top layer experiences tensile stress. The maximum tensile stress is observed at the starting of the scanning track. This is because of presence of maximum temperature gradient at the starting of the scanning because of
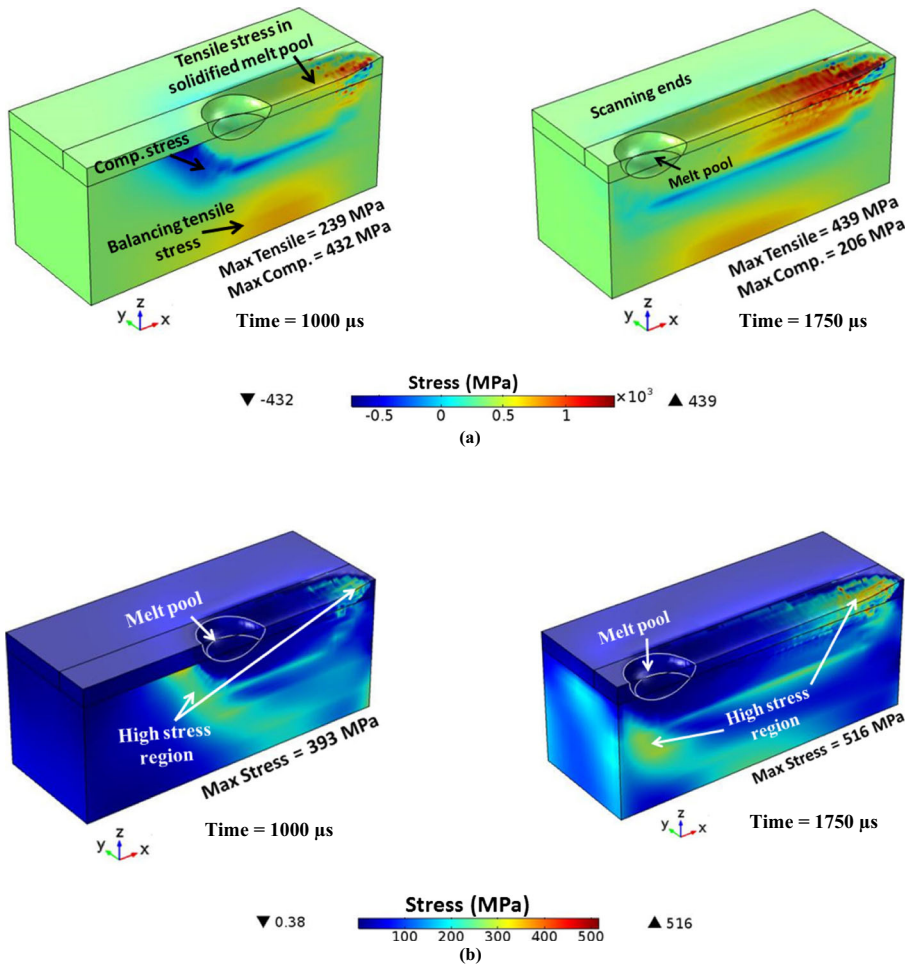
Fig. 7 (a) Stress (σ_{xx}) (b) von Mises stress field during the heating of the component

presence of low conductivity powder layer on both sides [11]. It can be noted that at the starting of the scanning, the stress field developed is non-uniform. This can be due to sudden change of the phase and hence material properties from powder material to the bulk solid material.

Figure 7 (b) presents the von Mises stress field during the heating of the component at time 1000 μs and 1750 μs. The magnitude of von Mises stress is low in the very neighbourhood of the melt pool due to loss of rigidity of the material at high temperature. High von Mises stress is observed at the starting of the scanning and at distance little away from the neighbourhood of the melt pool due to presence of rigidity in material at comparatively low temperature than in neighbourhood of the melt pool. The magnitude of the longitudinal component is observed considerably higher than the other components of the stress tensor [12]. Therefore, only the longitudinal component of the stress along with von Mises stresses is studied in this work.

Stress during Cooling Stage

Figure 8 shows the stress field developed during the cooling of the component at time 1850 μs and 4000 μs. The laser heat source is switched off at time 1750 μs and the melt pool will completely solidify at time 1850 μs. During the cooling, the top surface starts to cool down as soon as the laser is removed. Due to this, the top layer experience thermal contraction and tries to shrink. But the remaining material of the component does not allow it to shrink freely and hence there is tensile stress zone observed at the top of the component (Fig. 8). The material underneath the tensile stress zone experiences balancing compressive stress to maintain the equilibrium. Figure 9 depicts the variation of stress (σxx) along the depth at the centre and along the scanning direction at the end of cooling stage, i.e., at 4000 μs. Along the depth, the magnitude of tensile stress decreases up to 45 μm depth of the solid substrate after which the tensile nature of the stress will change to compressive. The maximum compressive stress lies in the just vicinity of the tensile stress zone after which its magnitude will get decreased (Fig. 9 (a)). Along the length the maximum magnitude of the tensile stress is observed at the starting of the scanned track because of high temperature gradient in this location (Fig. 9 (b)).

Figures 10 (a) and 10 (b) show the map of von Mises stress during the cooling of the component at 1850 μs and 4000 μs. It was pointed out in previous section that the component is not allowed to cool up to the room temperature in order to deposit the next powder layer over the pre-heated previous layer. Due to this reason, the von Mises stresses are little less at the end of the track which is at relatively high temperature than the already scanned track. Also, there is irregularity in the stress field at the interface of the powder and solid material. This can be due to sudden change of the material properties. The critical location of high von Mises stress is shown in Fig. 10 (c). At this location, there is introduction of plastic stress in the material and it will remain in the component as residual stress when the component is finally cooled down to the ambient conditions. Figure 11 shows the magnitude variation of von Mises stress along the depth at the center and along the scanning
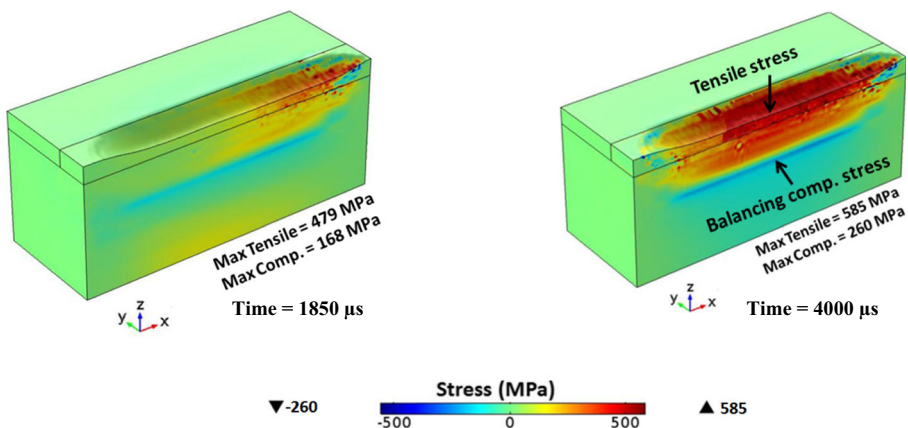

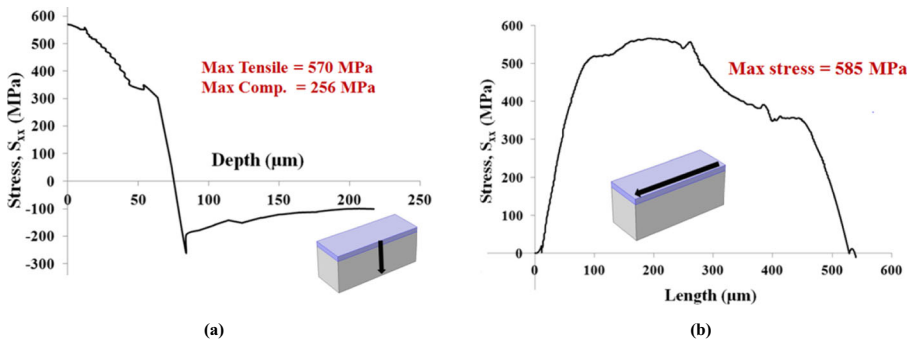Fig. 8 Stress (σ_{xx}) field during the cooling stage

Fig. 9 Stress (σ_{xx}) distribution (**a**) along the depth at the center (**b**) along the scanning direction at the end of cooling stage

direction at completion of cooling stage, i.e., at 4000 μs. Along the length, the highest magnitude of the thermal residual stress is found at the starting of the scanning track and retain up to some length after which the magnitude decreases due to loss of rigidity at comparatively high temperature (Fig. 11 (b)).
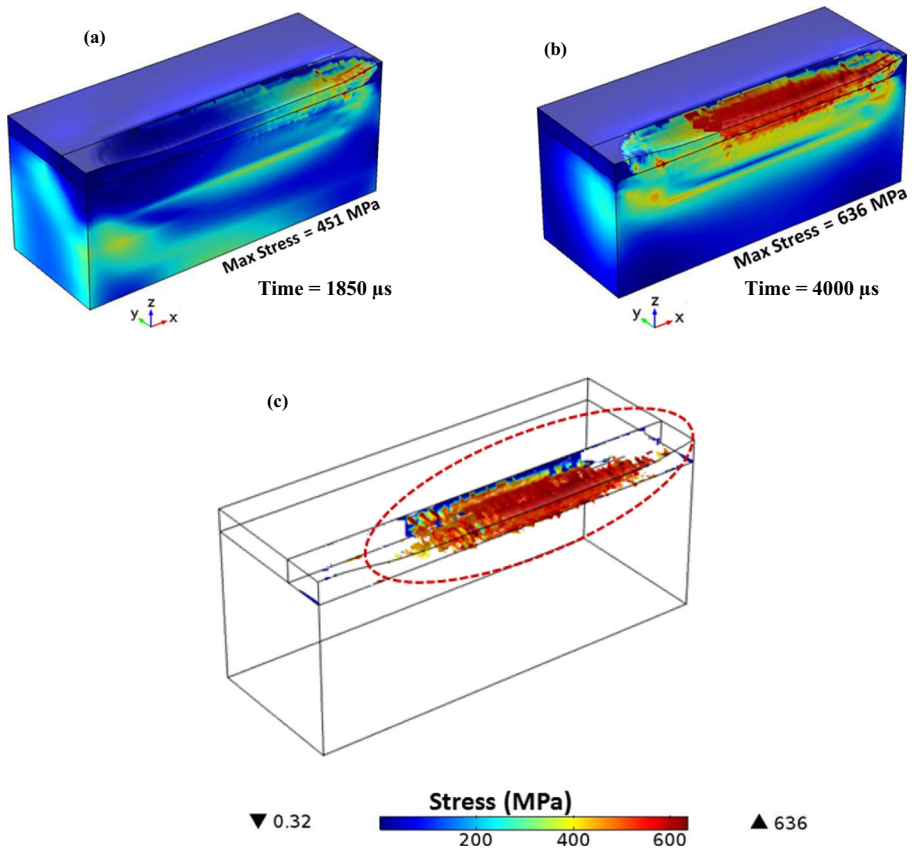

Fig. 10 von Mises stress field during the cooling stage (**a**) t = 1850 μs (**b**) t = 4000 μs (**c**) critical location of high von Mises stress
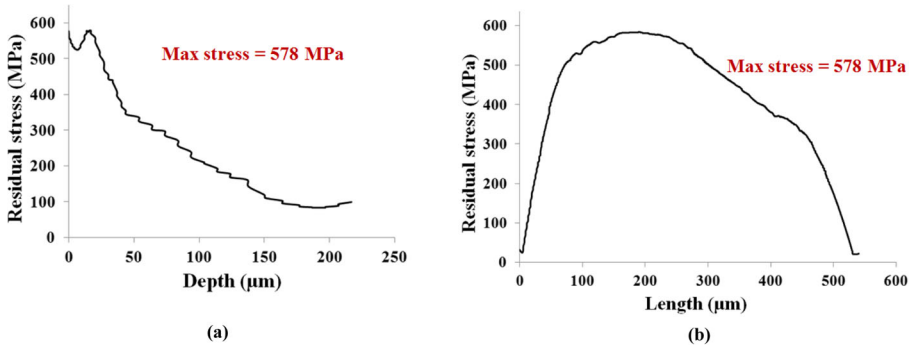
Fig. 11 von Mises stress distribution **(a)** along the depth at the centre **(b)** along the scanning direction at completion of cooling stage

Dependence of Stresses on Process Parameters

Cracking in the component is one of the major defects manufactured by selective laser melting technique. It happens when the magnitude of the residual stress in the component exceeds beyond a certain level. The magnitude of residual stress locked-in the component depends on various parameters, such as laser power, scanning speed of the laser, interaction time, scanning strategy and pre-heating of the solid substrate. Figure 12 shows the effect of important parameters on the magnitude of the residual stress along the scanning direction at top layer of the component. It is observed in Fig. 12 (a) that as we increase the power of the laser heat source, magnitude of the residual stress will increase. The scanning speed and the substrate temperature are kept constant as 250 mm/s and 293 K, respectively. The magnitude of maximum residual stress decreases by 29% as power of laser heat source decreases from 60 W to 25 W. It can be noted that, for 60 W laser heat source, the melt pool size is bigger. Therefore, the length of the processed powder track is also large. Due to this, magnitude of the stress is higher at the starting of the track. Also, it is observed in Fig. 12 (b) that as the scanning speed of the laser heat source is decreased, the magnitude of residual stress will increase due to increase in availability time of the heat source at the same place. The other parameters, i.e., power and substrate pre-heat temperature are kept constant at 40 W and 293 K. The magnitude of maximum residual stress decreases by 62%, as interaction time of laser heat source, decreases from 350 mm/s to 150 mm/s. Therefore, an appropriate combination of the laser power and scanning speed is recommended such that proper bond will establish between the layers and minimum residual stress will develop. Figure 12 (c) shows the variation of magnitude of residual stress with substrate pre-heating with constant laser power and scanning speed of 40 W and 250 mm/s. It is observed that as the pre-heating temperature of the solid substrate is increased, magnitude of the residual stress decreases. This is because the pre-heating helps to lower the steep temperature gradient, and as a result the residual stress reduces. The magnitude of maximum residual stress decreases by 41% as substrate is pre-heated up to 673 K from room temperature. But, the microstructure of the material will change with the heating of the substance which in result changes
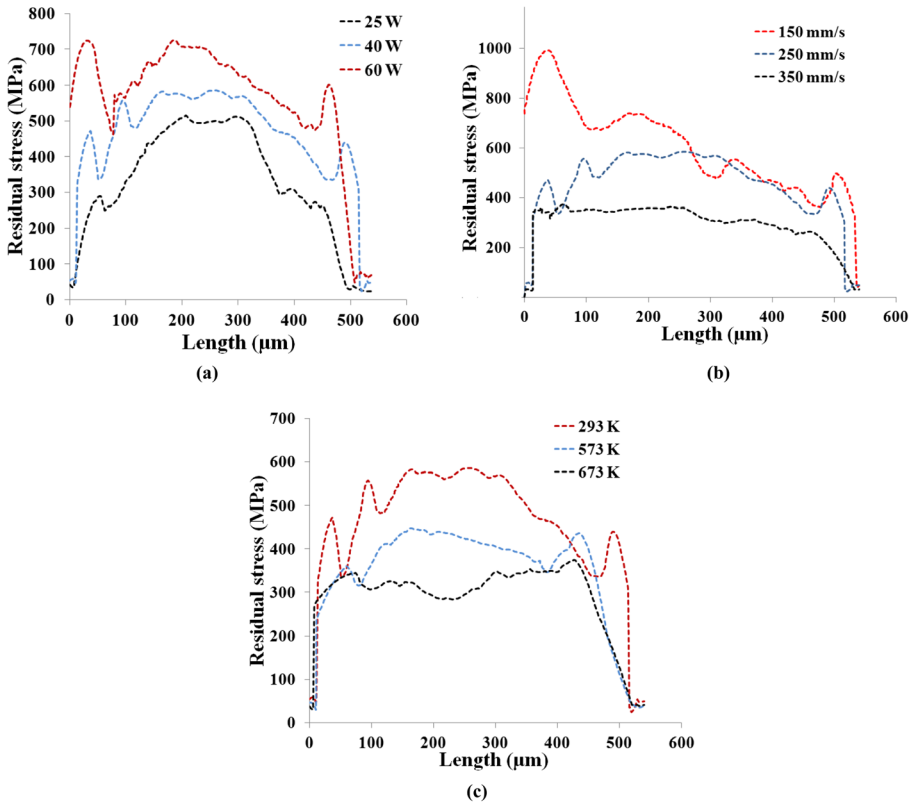
Fig. 12 Effect of (a) laser power (b) scanning speed (c) substrate pre-heat temperature on residual stress along the laser scanning direction

the material properties of the component. Therefore, pre-heating of the component is done according to the application of the component and its microstructural requirement.

Multi Track Laser Scan Simulations for Meso-Scale Stress Evolution

To understand the development of thermal field and resulting stress field multi-track scanning in SLM, a meso-scale model is developed. A 40 W laser heat source with spot radius of 26 μm with Gaussian type intensity distribution is used with scanning speed of 250 mm/s. The hatch space between the tracks is taken as 50 μm. Initially the domain is maintained at ambient temperature (293 K) before the scanning by laser heat source. The powder layer is scanned by alternate as well as uni-directional scanning strategy. The residual stress field developed after the completion of scanning and cooling of the component for both the scanning strategies are compared. Figure 13 shows the temperature maps during the scanning of powder bed by laser heat source by adopting the alternate scanning strategy. The highest temperature obtained is 4740 K. There is some re-melting takes place in the solid substrate in order to make good bonding between the solidified powder material and solid substrate (Fig. 13 (f)). After the completion of the cooling stage i.e. at 15 ms, the
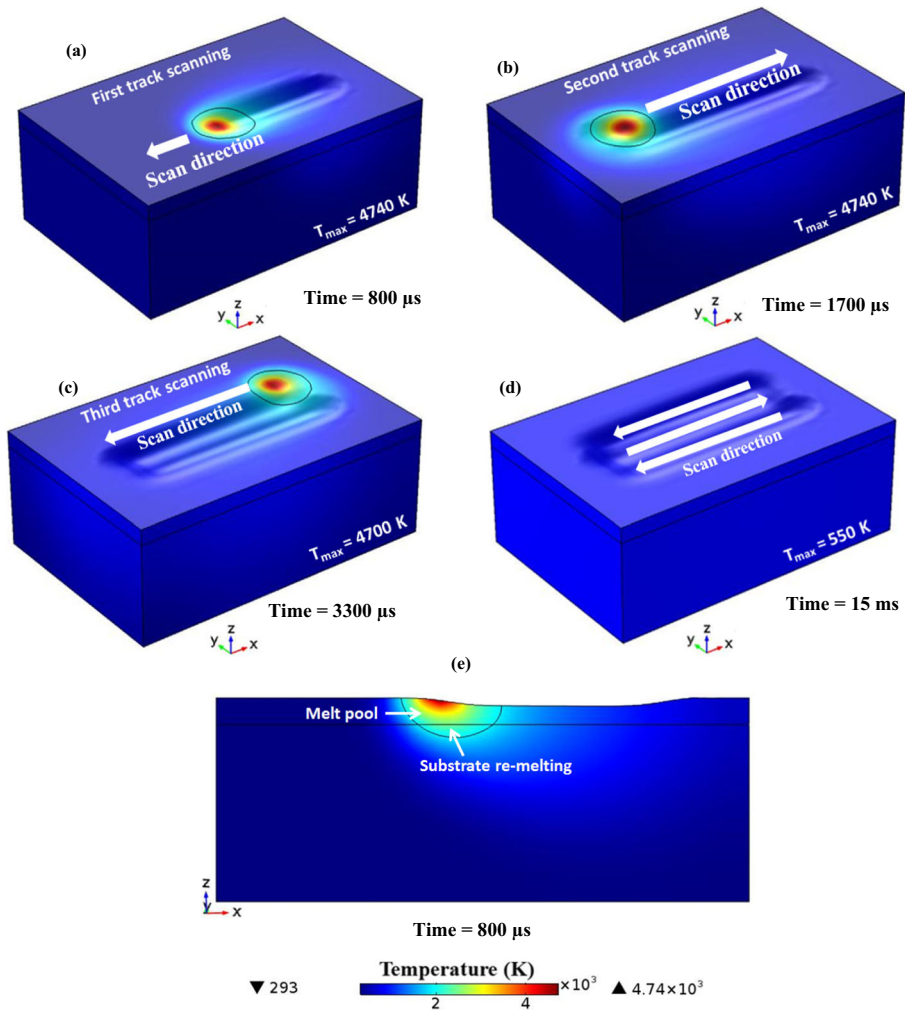
Fig. 13 Temperature field **(a)** 800 μs **(b)** 1700 μs **(c)** 3300 μs **(d)** 15 ms **(e)** cross-sectional view along the scanning direction during the first track scanning at 800 μs

component is cooled down due to convective and radiative losses up to 550 K temperature. The component was not cooled down up to the ambient temperature as new powder layer is deposited over the pre-heated solidified layer in SLM process to reduce the thermal stress.

Figure 14 shows the cross-sectional view of overlapped melt pools in different tracks in the transverse direction to the laser scanning as the solidified tracks would look be in reality. The temperature distribution at the top layer of the overlapping melt pools is superimposed. The melt pools for the different tracks at particular cross-section are superimposed to obtain the quantified visualization of hatch spacing. There is approximately 50% hatch spacing between the two scanned tracks which ensures proper bonding between the two tracks. It can be noted that the melt pools are bit distorted because of different amount of volume reduction at different time.
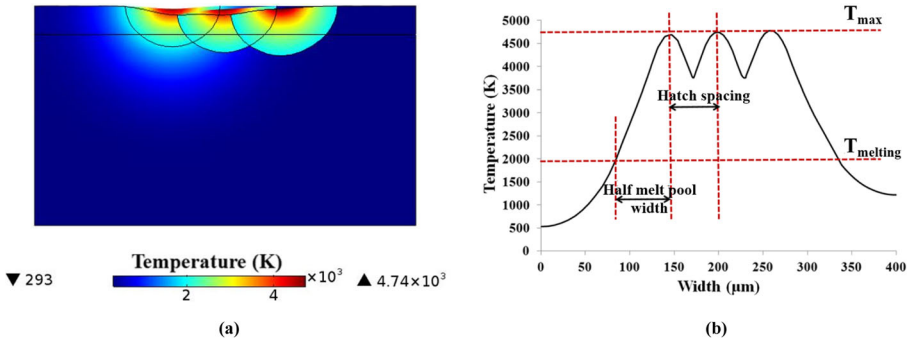
Fig. 14 Multi-track scanning results (a) Cross-sectional view of the melt pool in the various scan (b) temperature profile at the top surface for overlapped melt pools across the hatch

Figure 15 shows the material properties variation in the model with different phase of the material. There are three phase changes in SLM process i.e. the initial powder phase, the liquid phase and finally the solid phase at the top powder layer. In simulation, these phase
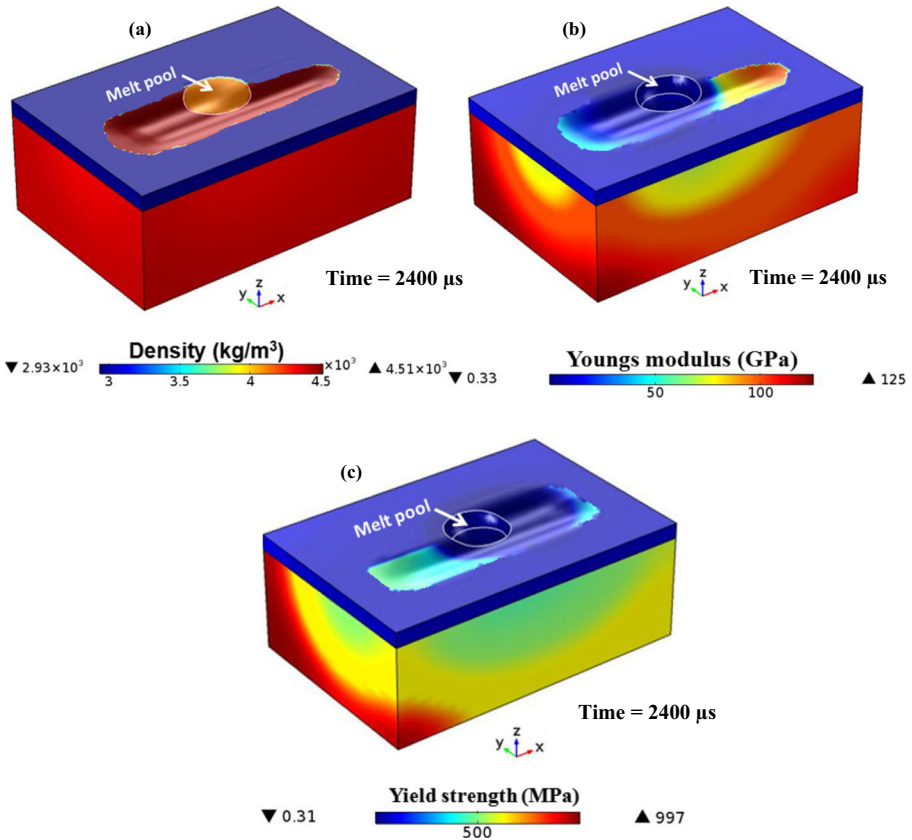

Fig. 15 Material properties variation **(a)** density **(b)** Youngs modulus **(c)** yield strength during laser scanning of the powder layer

changes are incorporated by the change in the material properties. The laser unaffected region has the properties of powder material like negligible rigidity and low density, the melt pool region has properties of liquid and solidified melt pool assumes the properties of bulk solid like high rigidity and density in the top layer. Also, during the scanning, the material in the neighbourhood the melt pool experiences low rigidity and low yield strength due to loss of rigidity at the high temperature (Fig. 16 (b) and Fig.16 (c)).

Figure 16 presents the σ_{xx} and von Mises stress field and the transverse cross-sectional view along the scanning direction after the completion of the cooling stage. The same trend, as in the micro-scale model, i.e., tensile stress in the top layer and balancing compressive stress underneath it, is observed here also. The scanning of the powder layer by adopting the alternate scan strategy will induce comparatively low temperature gradient as compare to uni-directional scan strategy. This is because in alternate scanning the temperature gradient induced is comparatively low because while moving from one track to another track, the laser will move to the location adjacent to the high temperature region. In uni-directional scan strategy, laser has to move on low temperature side while moving from one track to another and hence experience relatively high temperature gradient. Figure 17 presents the stress (σ_{xx}) field and von
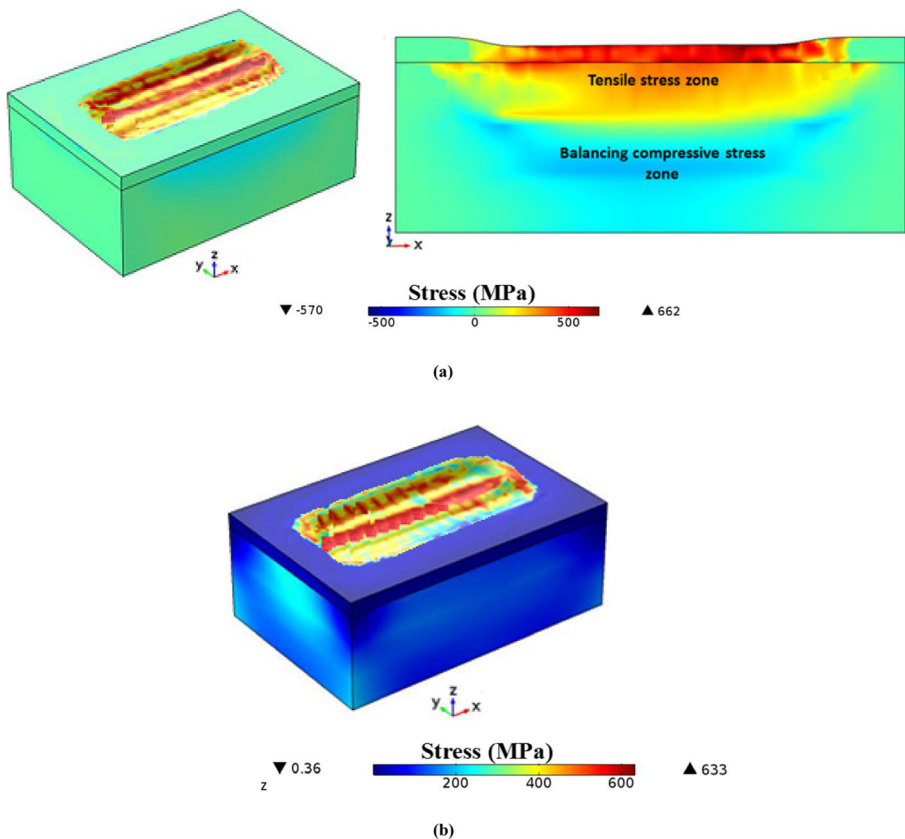

Fig. 16 (a) Stress (σ_{xx}) field and its cross-sectional view along the scanning direction (b) von Mises stress field for alternate scan strategy after the completion of the cooling stage
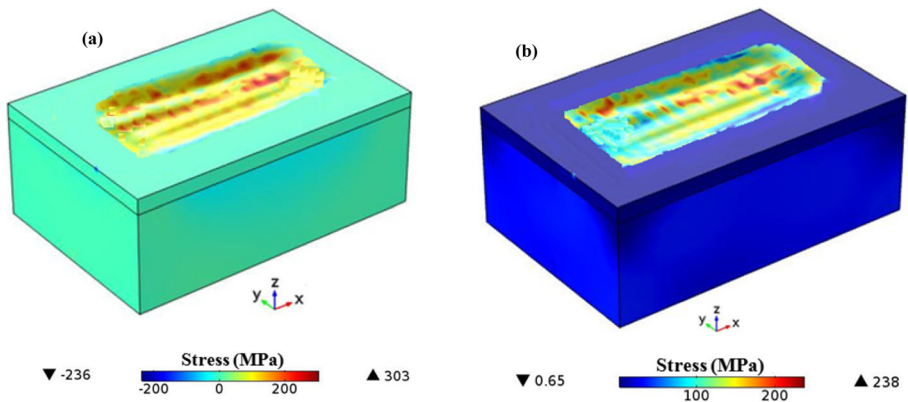
Fig. 17 **(a)** Stress (σ_{xx}) field **(b)** von Mises stress field for uni-directional scan strategy after the completion of the cooling stage

Mises stress field after the completion of the cooling stage for uni-directional scan strategy. It can be compared from Table 5 that the maximum magnitude of the residual stress in uni-directional strategy is 5% more as compared to the alternate scan strategy.

There are many factors which influence the magnitude of the thermal residual stress developed during the manufacturing of the component by selective laser melting technique. In the previous sections, it was concluded that the residual stress magnitude increases with increase in the laser power and by reducing the scanning speed. And, there is considerable reduction in the residual stress magnitude with the pre-heating of the solid substrate. It is observed from the meso-scale simulations, the alternate scan strategy developed less residual stress as compared to the uni-directional scan strategy. Therefore, for the particular component, there can be many sets of the optimum parameters which will develop minimum residual stress without hampering the quality of the process such as proper bonding between the powder layer and solid substrate. Figure 18 shows the residual stress in the domain by considering the one set of the optimum parameters for this model, i.e., 40 W laser power, 250 mm/s scanning speed, 673 K pre-heat temperature and alternate scan strategy. Table 5 compares the magnitude of the residual stress without adopting the optimum parameters and with adopting the one set of the optimum parameters. It can be observed that by adopting the optimum parameters, the magnitude of the thermal residual stress can be minimized considerably.

Table 5 Maximum residual stress for different process parameters

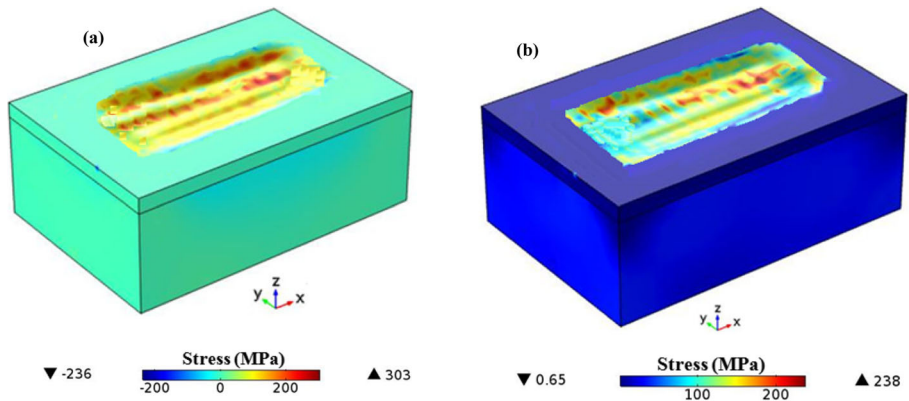| Laser power (W)	Scan speed (mm/s)	Substrate pre-heat temperature (K)	Scanning strategy	Maximum residual stress (MPa)
40	250	293	Alternate	633
40	250	293	Uni-directional	667
40	250	673	Alternate	238

Fig. 18 **(a)** Stress (σ_{xx}) field **(b)** von Mises stress field by adopting the set of optimum parameters after the completion of the cooling stage

Discussion

The high temperature gradient, due to localized heating of the powder layer laid over the solid substrate, is the main cause of origin of thermal stresses in the component [28]. It causes different volumetric expansion or contraction at different locations as thermal expansion coefficient is the function of temperature. Initially, as the scanning by the laser heat source starts, the powder gains heat from the heat source and try to expand. The powder in the neighbourhood region of the melt pool does not restrict the expansion as it is loosely held. Therefore, material can freely expand initially and there will be no stress generation. Further, there is formation of the melt pool at that spot due to increase of localized temperature above melting temperature of the material. The melt pool does not experiences any stress. As time goes on, size of the melt pool increases and melt pool reaches up to the solid substrate and some melting takes place in it too. The material just in the neighbourhood of the melt pool solid substrate is at high temperature and starts expanding. This expansion is restricted by surrounding substrate material. Therefore, the material just in the neighbourhood of the melt pool experiences compressive stresses and the surrounding material develop tensile stresses to balance the compressive stress and maintain the equilibrium [29]. When the laser heat source moves away with time, this region starts to cool down. The region affected by heat tries to shrink as its temperature decreases. But the surrounding material does not allow it to shrink freely and hence tensile stresses are developed in the solidified melt pool region. Again, compressive stress zone developed underneath it to balance tensile stress and maintain equilibrium in the component. These tensile stresses in top layer and balancing compressive stresses underneath it, remain locked-in the component as residual stresses, even after the component cools down completely. This phenomenon is schematically shown in Fig. 19.

The development of stresses in the powder bed during the SLM process at a fundamental level (track-scale) is not yet comprehensively reported in the previous work done in this field. The available literature on residual stress deals with its development after the complete cooling of the component. Although the simulated stress field is not directly validated, the validation of the thermal model can be
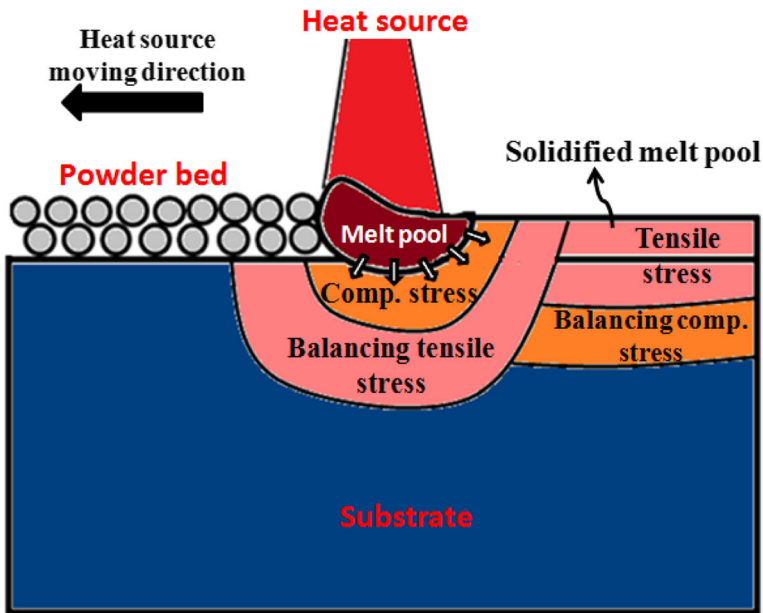
Fig. 19 Development of thermal stress during laser scanning

considered as a proof of the correct prediction of the stress field as stress development is caused by the temperature gradient. Also, it can be noted that the physical issues of the SLM process are quite comprehensively coupled in the present thermo-mechanical model. It can be noted that the coupling of volume reduction due to porosity in the powder layer during the selective laser melting for stress prediction has been numerically implemented only in a few literature [14, 15]. As the selective laser melting technique is widely growing in different industries, the results presented in this work can be useful as guidelines to minimize the unwanted thermal residual stresses. The optimum combination of laser power and laser scanning speed, the substrate pre-heating and adoption of alternate scanning over the uni-directional scanning are helpful to mitigate the residual stresses. Nevertheless, there is strong need of track-scale experimental studies under controlled conditions focusing at the development of stresses at the micro and meso-scale.

Conclusions

An investigation of track-level evolution of thermal field and resulting thermal stresses at micro scale and meso scale is performed for the deposition of single Ti6Al4V powder layer over the substrate by selective laser melting process. A 3D fully coupled FE thermo-mechanical model is developed, which incorporates powder-liquid-solid transition including melting and solidification, material properties which are dependent on temperature, reduction of volume of the porous powder layer during heating, and the stress evolution. The mechanical model incorporates plastic behaviour of the material and temperature dependent material properties. To minimize the track-level stresses, a range of parameters is also suggested. The conclusions of this study are:

- Typically, the area in the proximity of the melt pool along with the solid substrate up to depth of 115 μm experiences compressive stress during the heating stage and a zone of tensile stress to balance compressive stress is found underneath it up to the bottom fixed boundary.
- During the cooling stage, the already scanned powder layer away from the melt pool experiences tensile stress up to 25 μm depth of the substrate due to restricted thermal contraction and there is a balancing compressive stress zone underneath it.
- It was observed that thermal stress is highest (i.e., 636 MPa) at the starting of the scanning track due to highest temperature gradient at the starting of the scanning.
- The magnitude of maximum residual stress reduces by 29% with decrease in laser heat source power from 60 W to 20 W, and by 62% with increase in laser scanning speed from 150 mm/s to 350 mm/s. It is suggested to use suitable values of laser power and scanning speed for which minimum thermal residual stress will induce and proper bonding between the layers will be developed.
- The maximum value of residual stress reduces by 41% with the substrate pre-heating temperature of 673 K temperature than no substrate pre-heating.
- During multi-track scanning, the maximum value of residual stress reduces by 5% by adopting the alternate scanning over the uni-directional scanning.
- It is determined from this study that alternate scanning of the powder layer, with substrate pre-heating up to 400 °C and using laser power and scan speed of 40 W and 250 mm/s can be appropriate to minimize the track-scale residual stress for selective laser melting of Ti6Al4V.

References

1. Dutta, B., Froeas, F.: The additive manufacturing (AM) of titanium alloys. Met Powder Rep. **72**, 96–106 (2017)
2. Gokuldoss, P., Kolla, S., Eckert, J.: Additive manufacturing processes: selective laser melting, electron beam melting and binder jetting – selection guidelines. Mater. **10**, 672 (2017)
3. Gibson, I., Rosen, D., Stucker, B.: Additive Manufacturing Technologies. Springer-Verlag, New York (2015)
4. Ahmad, B., Veen, S., Fitzpatrick, M., Guo, H.: Residual stress evaluation in selective-laser-melting additively manufactured titanium (Ti-6Al-4V) and inconel 718 using the contour method and numerical simulation. Addi Manufac. **22**, 571–582 (2018)
5. Leuders, S., Thöne, M., Riemer, A., Niendorf, T., Tröster, T., Richard, H.A., Maier, H.J.: On the mechanical behaviour of titanium alloy TiAl6V4 manufactured by selective laser melting: fatigue resistance and crack growth performance. Int J Fatigue. **48**, 300–307 (2013)
6. Vastola, G., Zhang, G., Pei, Q.X., Zhang, Y.W.: Controlling of residual stress in additive manufacturing of Ti6Al4V by finite element modeling. Addit. Manuf. **12**, 231–239 (2016)
7. Shiomi, M., Osakadal, K., Nakamural, K., Yamashital, T., Abe, F.: Residual stress within metallic model made by selective laser melting process. CIRP Ann. **53**(1), 195–198 (2004)
8. Mercelis, P., Kruth, F.: Residual stresses in selective laser sintering and selective laser melting. Rapid Prototyp. J. **12**(5), 254–265 (2006)
9. Cheng, B., Shrestha, S., Chou, Y.: Stress and deformation evaluations of scanning strategy effect in selective laser melting. Addi. Manufac. **12**, 240–251 (2016)
10. Song, J., Wu, W., Zhang, L., He, B., Lu, L., Ni, X., Long, Q., Zhu, G.: Role of scanning strategy on residual stress distribution in Ti-6Al-4V alloy prepared by selective laser melting. Optik. **170**, 342–352 (2018)

11. Hussein, A., Hao, L., Yan, C., Everson, R.: Finite element simulation of the temperature and stress fields in single layers built without-support in selective laser melting. Mater & Des. **52**, 638–647 (2013)

12. Li, C., Liu, J.F., Fang, X.Y., Guo, Y.B.: Efficient predictive model of part distortion and residual stress in selective laser melting. Addi. Manufac. **17**, 157–168 (2017)

13. Li, Y., Zhou, K., Tan, P., Tor, S.B., Chua, C.K., Leong, K.F.: Modeling temperature and residual stress fields in selective laser melting. Int J Mech Sci. **136**, 24–35 (2018)

14. Li, Y., Zhou, K., Tor, S., Chua, C., Leong, K.: Heat transfer and phase transition in the selective laser melting process. Int J Heat and Mass transf. **108**(B), 2408–2416 (2017)

15. Tan, P., Shen, F., Li, B., Zhou, K.: A thermo-metallurgical-mechanical model for selective laser melting of Ti6Al4V. Mater. & Des. **168**, 107642 (2019)

16. Yilbas, B.S., Akhtar, S.S., Matthews, A., Karatas, C., Leyland, A.: Microstructure and thermal stress distributions in laser Carbonitriding treatment of Ti–6Al–4V alloy. Journal of Manuf Sci Eng. **133**, 021013–021011 (2011)

17. Wu, J., Wang, L., An, X.: Numerical analysis of residual stress evolution of AlSi10Mg manufactured by selective laser melting. Optik. **137**, 65–78 (2017)

18. Fan, Z. and Liou, F.: Numerical modeling of the additive manufacturing (AM) processes of titanium alloy. In: Amin, A.K.M. (Ed.) Titanium Alloys–Towards achieving enhanced properties for diversified applications, pp. 3–28. InTech (2012)

19. Welsch, G., Boyer, R., Collings, E.W.: Materials properties handbook: titanium alloys ASM international. Ohio. (1998)

20. Mills, K.C.: Recommended values of thermophysical properties for selected commercial alloys. Cambridge. (2002)

21. Parry, L., Ashcroft, I.A., Wildman, R.D.: Understanding the effect of laser scan strategy on residual stress in selective laser melting through thermo-mechanical simulation. Addit Manuf. **12**, 1–5 (2016)

22. Thummler, F., Oberacker, R.: An introduction to powder metallurgy. London. (1993)

23. Saxena, S., Sharma, R., Kumar, A.: A Microscale Study of Thermal Field and Stresses during Processing of Ti6Al4V Powder Layer by Selective Laser Melting Lasers in Manufacturing and Mater. Process., 1–31 (2018)

24. Verhaeghe, F., Craeghs, T., Heulens, J., Pandelaers, L.: A pragmatic model for selective laser melting with evaporation. Acta Mater. **57**, 6006–6012 (2009)

25. Buchbinder, D., Meiners, W., Pirch, N., Wissenbach, K., Schrage, J.: Investigation on reducing distortion by preheating during manufacture of aluminium parts using selective laser melting. J Laser App. **26**(1), 1–10 (2014)

26. Zaeh, M., Branner, G.: Investigations on residual stresses and deformations in selective laser melting. Prod Eng – Res Dev. **4**, 35–45 (2012)

27. Kruth, J., Deckers, J., Yasa, E., Wauthlé, R.: Assessing and comparing influencing factors of residual stresses in selective laser melting using a novel analysis method. Proceeding Institute of Mechanical Engineering Part B: Journal of Engineering Manufacture. **226**(6), 980–991 (2012)

28. Nickel, A.H., Barnett, D.M., Prinz, F.B.: Thermal stresses and deposition patterns in layered manufacturing. Mater Sci Eng A. **317**, 59–64 (2001)

29. Li, C., Wang, Y., Zhan, H., Han, T., Han, B., Zhao, W.: Three-dimensional finite element analysis of temperatures and stresses in wide-band laser surface melting processing. Mater. & Des. **31**, 3366–3373 (2010)